*Special Issue Article*

Structural Health Monitoring
2015, Vol. 14(2) 168–177

DOI: 10.1177/1475921714568406
shm.sagepub.com

# Development of an artificial neural network for source localization using a fiber optic acoustic emission sensor array

**Tao Fu[1], Zhichun Zhang[1], Yanju Liu[2] and Jinsong Leng[1]**

**Abstract**

An intelligent algorithm was developed based on backpropagation artificial neural network for the acoustic emission source localization. The established and trained methods of the algorithm were stated with the time difference of arrival detected by a fiber optic acoustic emission sensor array and the coordinates of acoustic emission source. The response characteristic of fiber optic acoustic emission sensor was calibrated with the commercial piezoelectric ceramic transducer (PZT) acoustic emission sensor, which provided that the fiber optic acoustic emission sensor was better suited to detect the low frequency of stress wave than the PZT sensor. Four fiber optic acoustic emission sensors were deployed in a square array in an aluminum plate for comparisons between different algorithms of source localization. Comparison results of acoustic emission source location provided that the intelligent algorithm improved the accuracy by reducing the nonlinear errors. For the anisotropic materials, a sensor array deployed in a diamond pattern was adopted. The velocities of stress waves in orthogonal directions were measured as the basic performance for both algorithms of source localization. Four sensors were integrated into a carbon fiber–reinforced polymer plate as a perfect structure for locating the acoustic emission source impacting on its surface. The experiment results provide that the maximum error is only 6.3 mm using the intelligent algorithm.

**Keywords**

Carbon fiber–reinforced polymer, structural health monitoring, source localization, fiber optic acoustic emission sensor, artificial neural network

## Introduction

In order to effectively detect defects of composites brought by production process, or to monitor the damage and failure of composite structures in real-time, more researchers have drawn attentions to the structural health monitoring (SHM) of carbon fiber–reinforced polymer (CFRP) composites. Especially, researchers recently have focused on guided wave inspection technique[1] and acoustic emission (AE) monitoring system[2–5] to achieve the continuous on-line monitoring goal[6], such as damage localization and identification. The primary goals of SHM are enhancing system reliability and safety and reducing maintenance cost.[7,8] But smart structures integrated with sensors and actuators into materials will be the tendency of development of SHM in the future.[9,10]

Traditional AE sensor is usually made of piezoelectric ceramic materials, and it is not suitable for embedding into fiber-reinforced composite structure as it is a bulky structure, which limits the development of smart structures. In this article, a type of fiber optic acoustic emission sensor (FOAES) is developed, which is able to be embedded in CFRP composite laminates. Multiple sensors are applied for the research of AE source localization on anisotropic plate-like composites

[1]Centre for Composite Materials and Structures, Harbin Institute of Technology (HIT), Harbin, P. R. China
[2]Department of Astronautical Science and Mechanics, Harbin Institute of Technology (HIT), Harbin, P. R. China

**Corresponding author:**
Jinsong Leng, Centre for Composite Materials and Structures, Harbin Institute of Technology (HIT), P.O. Box 3011, No. 2 YiKuang Street, Harbin 150080, P. R. China.
Email: lengjs@hit.edu.cn

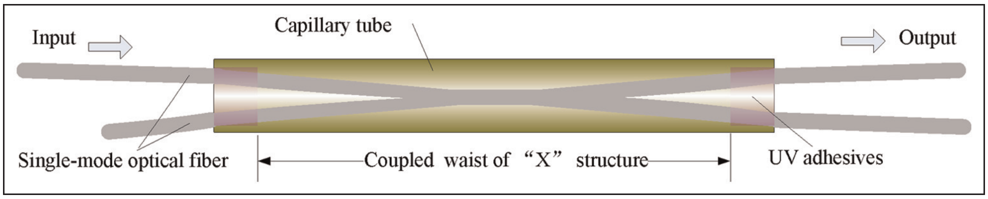


**Figure 1.** Schematic of FOAES.

structures. It is necessary to exactly determine the time of flight (TOF) from the AE source to multiple sensors for calculating the coordinates of AE source using the algebra algorithm. However, it can only locate the coordinates of AE source in isotropic material plate-like structures. Also, there is inevitable nonlinear error in the process of solving equation sets. To overcome the above weakness, an intelligent algorithm based on artificial neural network (ANN) is proposed for identifying AE source with embedded FOAES in CFRP plate. Artificial intelligent techniques are also researched and applied in SHM of composites, such as ANN[11–14] and genetic algorithm (GA).[15] But they are focused on identifying damage patterns of composites or optimized sensors. In this article, the algorithm of backpropagation (BP) ANN is created based on time difference of arrival (TDOA). It is essential for the algorithm to calculate a mass of TDOA from every AE source to every sensor of the sensor array according to velocities of stress waves propagating in the test plate. Then the accurate BP network is trained with the TDOA as inputs and the coordinates of AE source as outputs. AE source localization experiments were conducted in an isotropic aluminum plate with a square array. In an anisotropic material of CFRP plate, AE sources were located in the area of a diamond array. All measurement results were calculated using the conventional algebra algorithm and the new developed intelligent algorithm of BP neural network, which proved that the development of the neural network was more accurate.

## Principle of methodology

### *FOAES*

The FOAES used for AE source location was prepared with fused tapered optical fiber coupler. Two single-mode optical fibers are coupled at the waist shaping an "X" structure as presented in Figure 1. To keep the fiber structures straight, undamaged, and clean, a capillary tube is selected for fixing the coupled fibers with ultraviolet (UV) adhesives.

When the FOAES is employed for monitoring AE signals, it is surface-mounted on or embedded into test structures. Once a transient stress wave is generated from AE source in the solid structures, it will propagate to the FOAES and drive the sensor's capillary tube and optical fiber vibration. Vibration of optical fibers in the capillary changes the coupling ratio of light intensity along the coupled area. The outputs of optical power vary with the changes in the coupling ratio. When the input of optical power is $P_0$, the output of optical power is expressed as[16,17]

$$\Delta P(l,t) = 2P_0\bar{C}\varepsilon_0 l\left[\sin\left(\frac{\pi l}{\Lambda}\right)/\left(\frac{\pi l}{\Lambda}\right)\right]\cos\left(\frac{\pi l}{\Lambda} - 2\pi f t\right) \tag{1}$$

where $\varepsilon_0$ is the effective strain amplitude and depends on the acoustic power; $\Lambda$ and $f$ correspond to the wavelength and frequency of the Lamb wave, respectively.

Any one output was able to express the information of the AE event, which was analyzed with the optical waveguide method and computer simulations.[18] To verify the FOAES has an excellent response characteristic to stress waves in CFRP laminates, a commercial PZT AE sensor and a transducer were employed for calibrating the amplitude–frequency response. The detailed performance characteristics of the two sensors are listed in Table 1. The FOAES has a narrower range of frequency response than the PZT senor, which is between 20 and 180 kHz. The peak-to-peak voltage reaching to 0.46 V at the frequency of 50 kHz proves that the FOAES is more sensitive to the signals of low frequency than the PZT sensor. The signal-to-noise ratio (SNR) of the FOAES is better than that of the PZT in the low-frequency range, which benefits to the identification of the TOF.

### *Algebra algorithm of AE source localization*

Usually, no less than three sensors are necessary for planar impact or damage localization in isotropic material plate-like structures. Four sensors are always employed for measuring the TDOA from the source to every sensor, because the propagation velocity of stress wave cannot be exactly determined. Then a set of nonlinear equations is built up to estimate the coordinates of the source. The algebra algorithms of a square array and a diamond array are analyzed as shown in Figure 2. The type of distribution array and its solution

**Table 1.** Comparative evaluation of the performance characteristics of sensors.

| | Frequency (kHz) | Voltage (V) | SNR (dB) | Rang of frequency (kHz) |
|---|---|---|---|---|
| PZT sensor | 170 | 0.27 | 23 | 40–310 |
| FOAES | 50 | 0.46 | 31 | 20–180 |

SNR: signal-to-noise ratio; FOAES: fiber optic acoustic emission sensor.

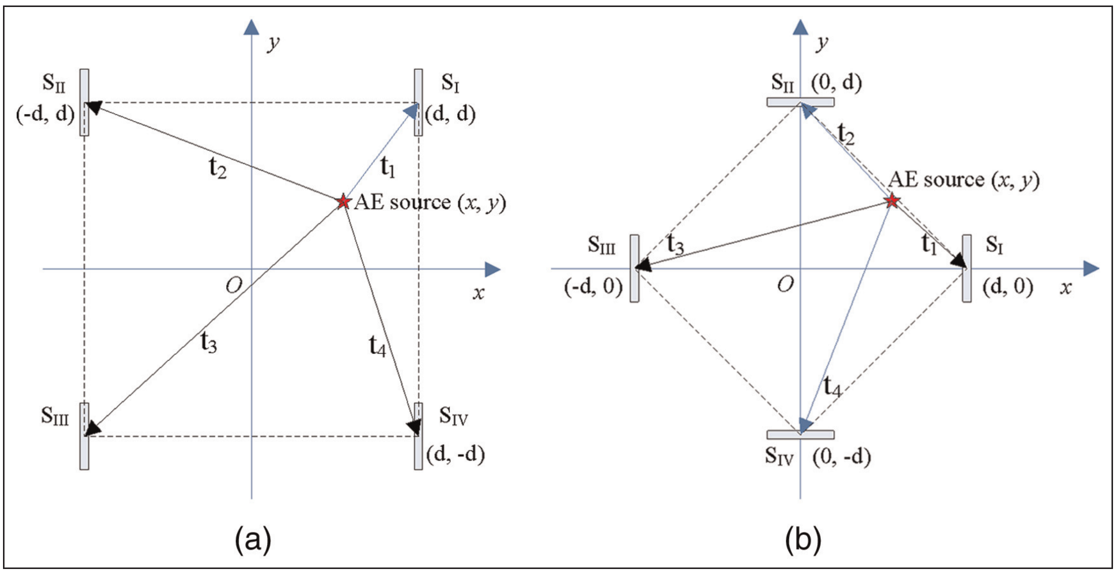


**Figure 2.** Schematic illustration of algorithms with (a) the square array and (b) the diamond array.

method depend on the performance of the materials. The square array is useful for isotropic material plate-like structures. For anisotropic material structures, an alternative method with a diamond array is proposed based on two sets of hyperbolic curves. The AE source in the area with the boundary of dotted line can be predicted by the algorithm according to the TDOA.

When the four sensors are distributed as a square array, the TOF from the AE source to every sensor is $t_i$. The coordinates of the unknown AE source $(x, y)$ and the fixed sensors can be expressed with the TOF and velocity

$$(x-x_i)^2+(y-y_i)^2=v^2t_i^2 \tag{2}$$

where $i$ is defined as the sequence number of sensor. When the TOF from the AE source to the first sensor $(t_1)$ is considered as the reference, the coordinates of AE source can be expressed with the TDOA from the AE source to other sensors

$$\begin{cases} (x-a)^2+(y-a)^2=v^2t_1^2 \\ (x+a)^2+(y-a)^2=v^2(t_1+\Delta t_2)^2 \\ (x+a)^2+(y+a)^2=v^2(t_1+\Delta t_3)^2 \\ (x-a)^2+(y+a)^2=v^2(t_1+\Delta t_4)^2 \end{cases} \tag{3}$$

where $v$ is the propagation velocity in an isotropic plate. $\Delta t_2=t_2-t_1$, $\Delta t_3=t_3-t_1$, and $\Delta t_4=t_4-t_1$ are defined as TDOA among the second, third, fourth, and the first sensors. The solutions of the nonlinear equation set can be solved in different methods. Su et al.[19] eliminated the reference time $t_1$, obtaining the solutions using three TDOAs and a constant velocity

$$\begin{cases} x=\dfrac{v^2\Delta t_2(\Delta t_3-\Delta t_4)(\Delta t_3+\Delta t_4-\Delta t_2)}{4a(\Delta t_2+\Delta t_4-\Delta t_3)} \\ y=\dfrac{v^2\Delta t_4(\Delta t_3-\Delta t_2)(\Delta t_2+\Delta t_3-\Delta t_4)}{4a(\Delta t_2+\Delta t_4-\Delta t_3)} \end{cases} \tag{4}$$

The theoretical coordinates can be obtained in ideal conditions. However, three TDOAs always inevitably exist with errors during actual measurement. The solutions will have errors as they are solved according to the TDOA with errors. The errors of the solutions do not linearly fit with the errors of the TDOA, which can be defined as nonlinear error.

When the four sensors are distributed as a square array, $\Delta t_{13}$ and $\Delta t_{24}$, two TDOAs measured by two pairs of FOAESs that were configured in a diamond array as shown in Figure 2(b). The normal hyperbolic equation is $(x^2/a^2)-(y^2/b^2)=1$, where $a^2+b^2=d^2$, $a = v\times\Delta t/2$, $v$ is the velocity of Lamb wave, $\Delta t$ is the

TDOA, and $d$ is the position coordinate of FOAES. Therefore, two pairs of FOAESs on $x$-axis and $y$-axis established two pairs of hyperbolas which were expressed as $(x^2/a_1^2)-(y^2/b_1^2)=1$ and $(y^2/a_2^2)-(x^2/b_2^2)=1$, where $a_1 = v \times \Delta t_{13}/2$, $b_1^2=d^2-a_1^2$, $a_2 = v \times \Delta t_{24}/2$, and $b_2^2=d^2-a_2^2$; we obtain $x^2=(a_2^2+b_1^2)/((b_1^2/a_1^2)-(a_2^2/b_2^2))$ and $y^2=(a_1^2+b_2^2)/((b_2^2/a_2^2)-(a_1^2/b_1^2))$. The velocity of acoustic wave propagation as a constant value is considered. However, in composite laminates as anisotropic materials, the velocity depends on the fiber orientation of CFRP plate.[20] Therefore, to improve the measurement accuracy, velocities on $x$-axis and $y$-axis are introduced to the hyperbolic location algorithm, and the position coordinates can be expressed as

$$x=\pm\sqrt{\frac{a_2^2+b_1^2}{\frac{b_1^2}{a_1^2}-\frac{a_2^2}{b_2^2}}},\quad y=\pm\sqrt{\frac{a_1^2+b_2^2}{\frac{b_2^2}{a_2^2}-\frac{a_1^2}{b_1^2}}} \tag{5}$$

where $a_1 = v_1 \times \Delta t_{13}/2$, $b_1^2=d^2-a_1^2$, $a_2 = v_2 \times \Delta t_{24}/2$, and $b_2^2=d^2-a_2^2$; $v_1$ and $v_2$ are the respective velocities in 0° and 90° orientation. The positive or negative value of $x$ was determined by $\Delta t_{13} = t_3 - t_1$, where $t_1$ is the arrival time from AE source to sensor I and $t_3$ is the arrival time from AE source to sensor III. Similarly, the positive or negative value of $y$ was determined by $\Delta t_{24}$ that was the TDOA between AE source to sensor IV and sensor II.

## Intelligent algorithm of BP neural network

BP neural network is widely used due to its more scientific training rules. In the supervised training process, the network weights and thresholds are constantly adjusted to minimize the output error of the network. As the nonlinear mapping ability of BP network is very powerful, three layers of network can realize the mapping between any inputs and expected outputs.[21] A hidden layer of BP network was selected to identify the location of the AE source, due to the advantages of simple structure and high efficiency.

Large input data and expected data for training the neural network are prepared for constructing a "black box," which can present regularly relationships between the inputs and the outputs of the network. In this article, the AE source location in plate-like structure was monitored by FOAES, based on TDOA from the AE source to different sensors. Therefore, the input data of the neural network are TDOA, and the output data are the coordinates of the AE source, which constitute the training sets. The process of establishment for training sets is shown in Figure 3, including the following steps:

*Step 1*. Measure propagation velocities of stress waves in different directions and set up a relationship between the propagation velocity and the propagation directions, $v = f(\theta)$.

*Step 2*. Mesh the testing structures, getting $m \times n$ intersections, coordinates of which are $(x_p, y_p)$, $p = 1, 2, \ldots, m \times n = T$. A simple plate structure is uniformly divided grid.

*Step 3*. The distance of all intersections on the grid to each sensor is calculated and presented as $l_p{}^i$. It can be obtained as

$$l_p{}^i=\sqrt{\left(x_p-x^i\right)^2+\left(y_p-y^i\right)^2} \tag{6}$$

where $i = 1, 2, \ldots, S$ is the $i$th sensor. At the same time, the angles of all the intersections to each sensor in the coordinate system are calculated as

$$\theta_p{}^i=\arctan\left(\frac{y_p-y^i}{x_p-x^i}\right) \tag{7}$$

*Step 4*. The calculated direction angle is substituted into the velocity function $v = f(\theta)$. Then the propagation velocity of stress wave from every intersection to every sensor is calculated as

$$v_p{}^i=f\left(q_p^i\right) \tag{8}$$

*Step 5*. The time of stress wave from every intersection to every sensor can be estimated with the relative distance and velocity

$$t_p{}^i=\frac{l_p{}^i}{v_p{}^i} \tag{9}$$

The important information for the training of ANN is collected in this step. Due to the AE source localization experiment, the physical quantities of time differences are usually directly measured. The time difference is first considered as the input vector of the neural network, in the process of ANN training.

*Step 6*. Determine the neural network input layer and output layer, namely, the training sample. According to the arrival time of stress wave $t_p{}^i$, taking the first sensor as the standard, the TDOA measured by other sensors can be obtained

$$\Delta t_p{}^i=t_p{}^i-t_p{}^1 \tag{10}$$

Obtain the matrix $S - 1 \times T$

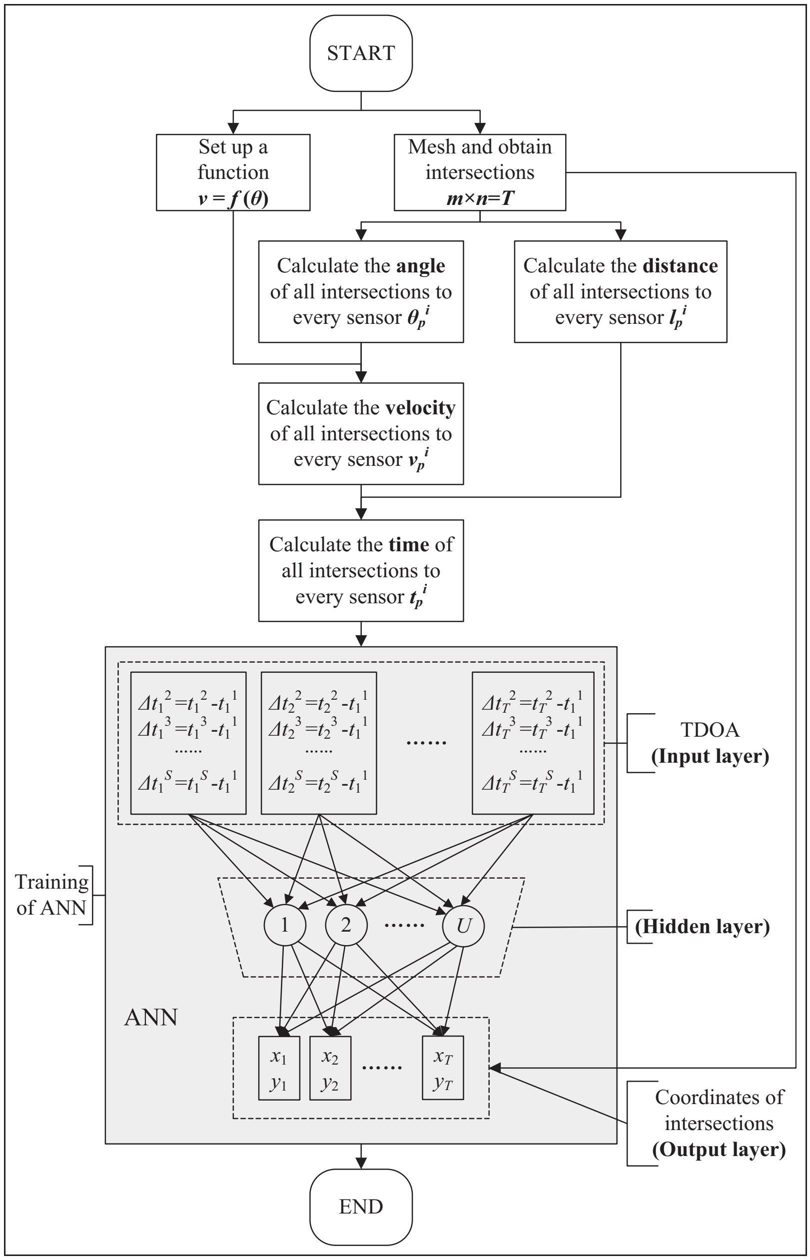


**Figure 3.** Source localization method based on artificial neural network.

$$\begin{bmatrix} \Delta t_1{}^2 = t_1{}^2 - t_1{}^1 & \Delta t_2{}^2 = t_2{}^2 - t_2{}^1 & \ldots & \Delta t_T{}^2 = t_T{}^2 - t_T{}^1 \\ \Delta t_1{}^3 = t_1{}^3 - t_1{}^1 & \Delta t_2{}^3 = t_2{}^3 - t_2{}^1 & \ldots & \Delta t_T{}^3 = t_T{}^3 - t_T{}^1 \\ \ldots & \ldots & \ldots & \ldots \\ \Delta t_1{}^S = t_1{}^S - t_1{}^1 & \Delta t_2{}^S = t_2{}^S - t_2{}^1 & \ldots & \Delta t_T{}^S = t_T{}^S - t_T{}^1 \end{bmatrix}_{(S-1)\times T} \quad (11)$$

In the matrix, every column of data is considered as one input vector. There are totally $T$ input vectors, which are relative to output vectors ($x_p$, $y_p$).

## Experiment setup and procedure

### *Experiment setup*

The experiment setup is shown in Figure 4: the signal generator is abandoned and the FOAES interrogator proves multi-channels for the FOAES array as shown in Figure 4(a). Four black thick lines in Figure 4(b) and (c) are FOAESs, which are distributed as a square array and a diamond array. The small circles represent the locations of AE source as test points.

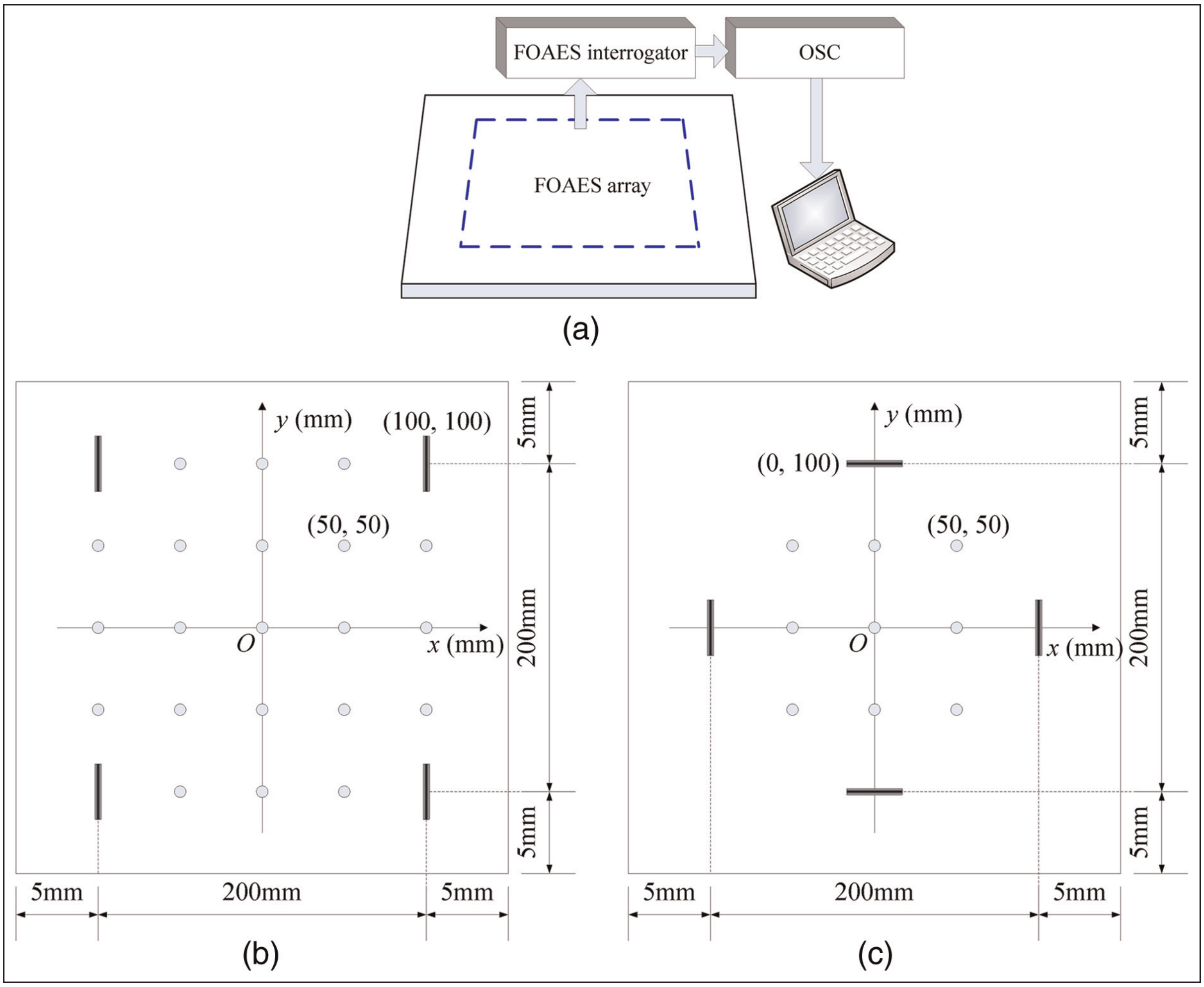


**Figure 4.** (a) Experiment setup, (b) positions of sensors in the square array, and (c) the diamond array in the coordinate system.

### *Propagation velocities of stress wave in CFRP plates*

The algorithm of impact source identification requires information of propagation velocities. The velocity profile was determined by the method of measuring TDOA. Figure 5 presents the propagation velocity profiles of stress waves in the aluminum plate ($300 \times 300 \times 1.8\ mm^3$) and the CFRP plate ($300 \times 300 \times 4.0\ mm^3$, $[0°/90°]_{7S}$). The velocities of stress waves propagating in the aluminum plate are uniform in all directions shown as red "•," and the average velocity is 1.321 km/s shown as green line in Figure 5. However, the velocities of stress waves measured by the embedded diamond array depend on propagation directions, which have the same trend as the velocity of the Lamb wave (A0 mode).[22] The velocities on $x$-axis and $y$-axis are 1.316 and 1.147 km/s, respectively. The velocities in other direction (green "▲" in Figure 5) are between the two extreme values, which are fitted as an ellipse curve (green line). The velocities on the green line employed for calculating TDOA was calculated, because the velocity on any direction was obtained easily and convenient for training the ANN.

### *Design and training results of BP neural network*

The operation efficiency and the accuracy of the neural network depend on hidden layer, and the most important is to choose the optimal number of neurons. If the number of neurons in the hidden layer is not enough, not only characteristic information collected from the training sets of the neural network are partial but also some expected outputs are easy to fall into local minimum value, getting the large training error. If there are too many neurons, the neural network in training

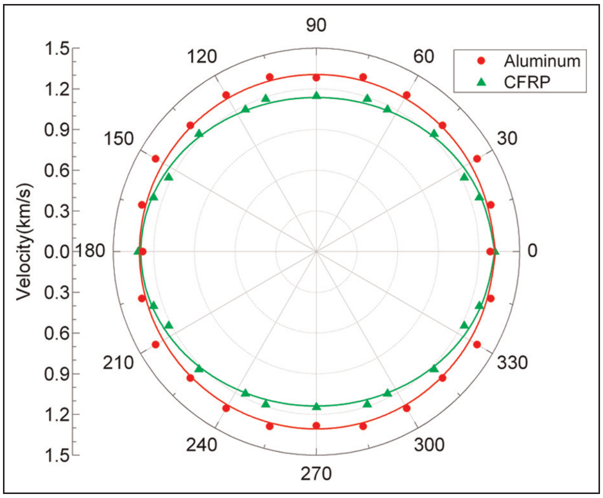


**Figure 5.** Propagation velocity profiles of stress waves in the aluminum plate and the CFRP plate.

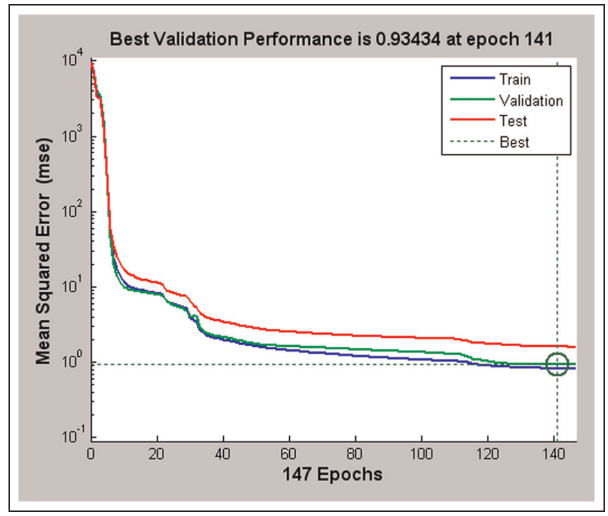


**Figure 6.** Relationships between the MSE of neural network and epochs.

process matches excessively, which affects the efficiency of the training at the same time, may not get the best training results. How to determine the optimal number of neurons in hidden layer is difficult. There are three kinds of formula for estimating the number of neurons

$$H = 2I + 1 \tag{12}$$

$$H = \sqrt{I + O} + a \quad a \in [1, 10] \tag{13}$$

$$H = \log_2 I \quad I \in [0.02I, 4I] \tag{14}$$

where $H$ is the number of neurons, $I$ is the dimension of the input vector of input layer, $O$ is the dimension of the input vector of input layer, and $a$ is constant. However, in order to design an ANN of accurate output value, it is best to compare their experiment number and increase the number of neurons, expanding the scope of the comparison, to determine the best network. The judgment standard for the best BP network is the mean square error (MSE), which refers to the output value and expectations exist deviation to neural network training process and can be expressed as

$$S = \sum_{i=1}^{n} \sqrt{\frac{(x_i - X_i)^2 + (y_i - Y_i)^2}{2}} \tag{15}$$

where $(x_i, y_i)$ is the $i$th output coordinates, $(X_i, Y_i)$ is the relative expected, and $n$ is the number of samples. The smaller the MSE, the more accurate the output value of neural network.

*FOAESs deployed in a square pattern.* Mash the square area into 200 mm $\times$ 200 mm grid spacing of 10 mm, obtaining 441 intersections, of which the arrival time to four fiber AE sensors are calculated as $T_1$, $T_2$, $T_3$, and $T_4$. When the four sensors were distributed as a square area, there were three input neurons and two output neurons in the BP network. A neural network with square array can get $441 \times 3$ $\Delta T_2 = T_2 - T_1$, $\Delta T_3 = T_3 - T_1$, and $\Delta T_4 = T_4 - T_1$. In all, 441 TDOAs $[\Delta T_2, \Delta T_3, \Delta T_4]'$ and 441 coordinates of intersections $[x, y]'$ are considered as three-dimensional input vectors and output vectors of training set, respectively. The number of hidden neurons is necessary to be increased because experimentation proceeds from 1.5 times of input neurons.

To set up a training set of an ANN, a rule of propagation velocities must be built up. According to the measurement results, a circle curve was fitted, which presented that propagation velocity of stress wave was averaged as 1.321 km/s. According to the above method of training set for ANN, the theory TDOA of stress wave was calculated as the training input vector. In the process of optimizing the number of hidden neurons, they were increased from 5 to 20. When the number of hidden neurons is 7, the neural network reaches a steady state after iterative 141 times and the minimum MSE is 0.93 as shown in Figure 6.

BP neural network is trained according to the TDOA of stress wave as training sets, and its results match the targets of AE source localization as shown in Figure 7. There are small errors at the boundary points of the square, and the maximum error is only 5.1 mm.

*FOAESs deployed in a diamond pattern.* When the sensor array is distributed in a diamond pattern, two pairs of TDOAs measured by sensors are presented as $\Delta T_{13} = T_3 - T_1$ and $\Delta T_{24} = T_4 - T_2$, which are two-dimensional vectors $[\Delta T_{13}, \Delta T_{24}]'$ of the network

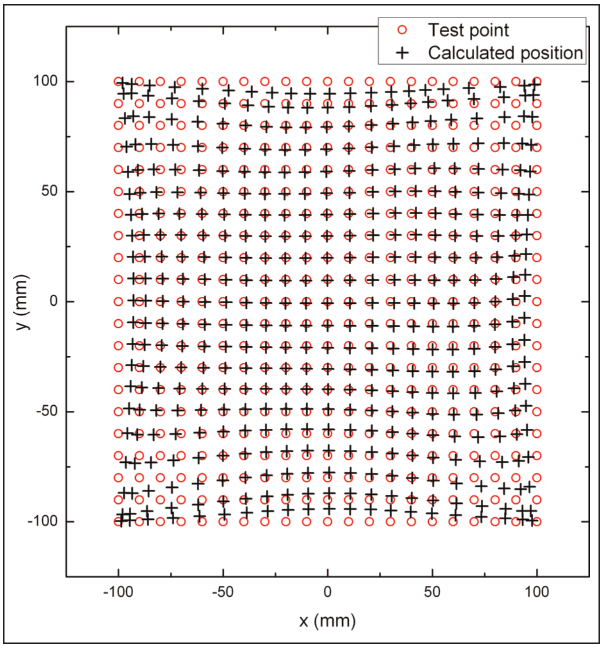


**Figure 7.** Training results of neural network with seven neurons.

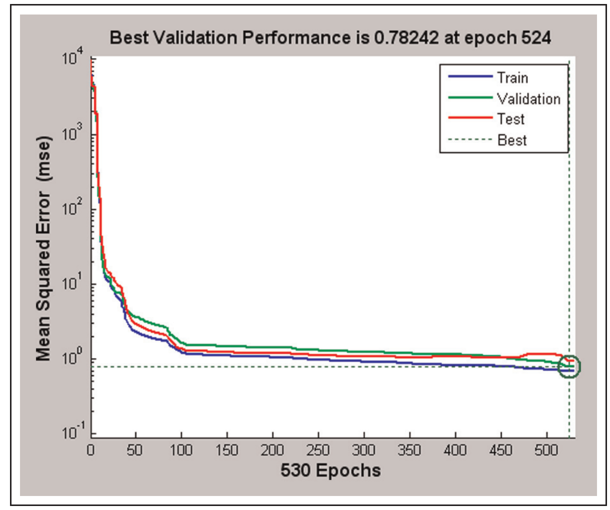


**Figure 8.** Relationships between the MSE of neural network and epochs.

input training sample. Output vector of the training set is composed of AE source coordinates of two-dimensional vector $[x, y]'$. The number of hidden neurons was determined with validations from 3. When the number of neurons is 18, after 524 iterations, training the output value and expectation of the MSE reduced to the minimum value of 0.782 as shown in Figure 8. Training results of BP neural network for the test points gridded in the area of the sensor array are shown in Figure 9. Compared with the results of the square array, almost all the calculated coordinates of the test points map the AE source location.

## Results and discussions

### *FOAESs distributed as a square array*

The experiment of AE source localization in the aluminum plate as isotropic material was implemented with the square array. Both algebra algorithm and intelligent algorithm based on BP neural network were adopted. Figure 10 shows the results of test points calculated by the algebra algorithm, most of which are much far from the actual AE source location with more nonlinear errors.

When the well-trained BP network is used to calculate the AE source location, all the test points coordinates are shown in Figure 11. There are only 5 of the 21 test points with more errors, and the maximum error is 10.6 mm, which does not exceed 5.3% relatively to the

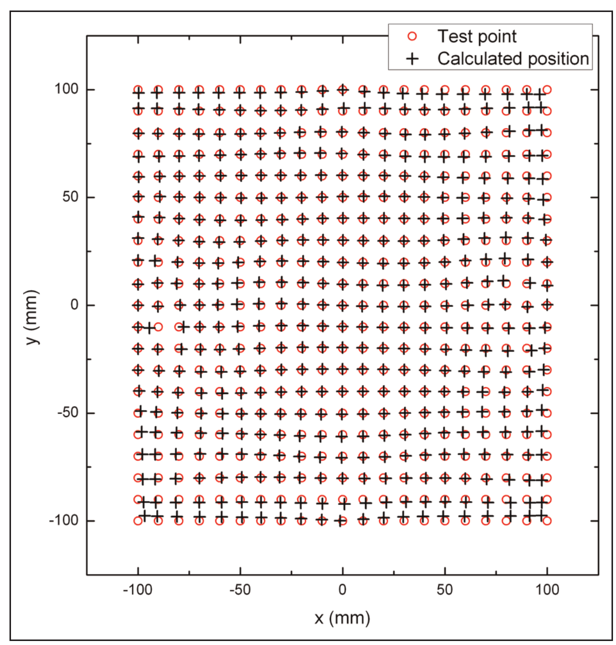


**Figure 9.** Training results of BP neural network for the diamond array.

measurement area. Compared with the above results of algebra algorithm, the algorithm of BP ANN is more accurate and stable in the global area.

### *FOAESs distributed as a diamond array*

The CFRP plate embedded with FOAESs was tested for location the impact source on the plate. Nine representative testing points in the CFRP plate were

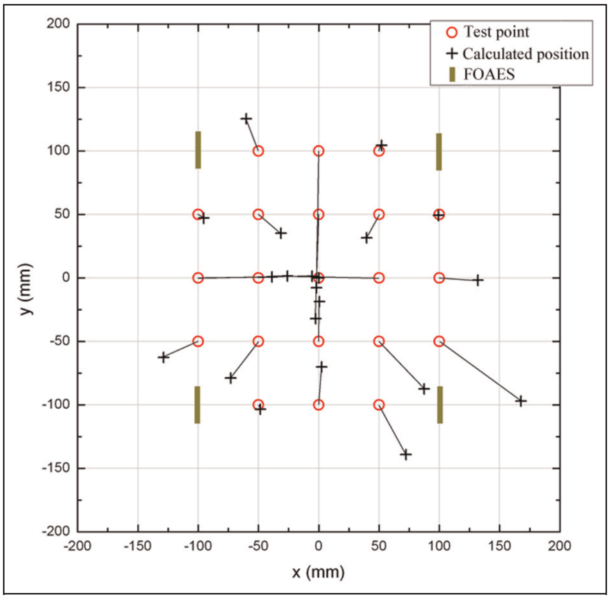


**Figure 10.** AE source localization results in an isotropic plate using the algebra algorithm.

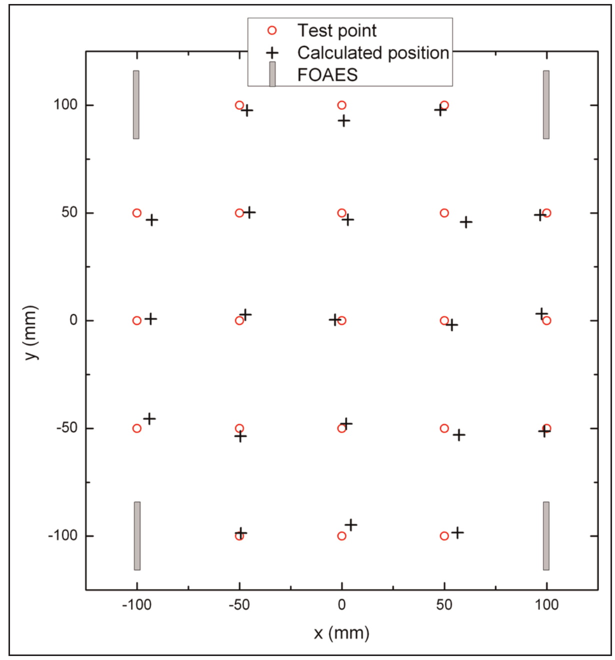


**Figure 11.** AE source localization results using the intelligent algorithm of BP neural network.

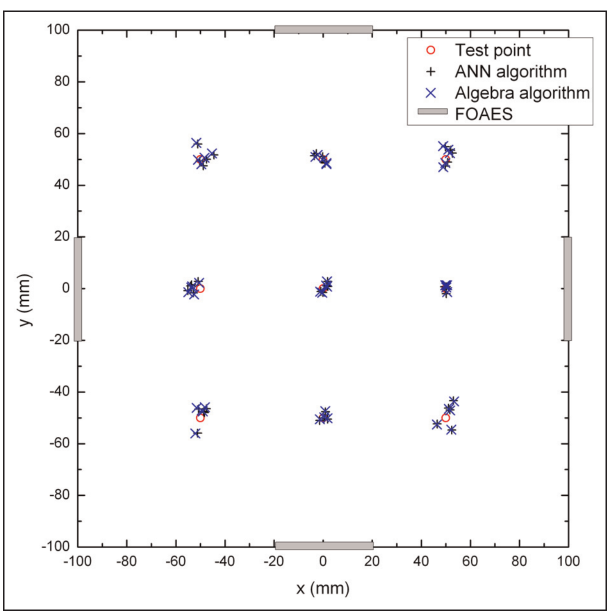


**Figure 12.** AE source localization results in the CFRP plate.

impacted with a steel ball repeatedly. At the same time, FOAESs detected the stress wave from the impact source, and the measurement system identified the arrival time from every sensor and calculated the coordinate of the impact source using the algorithm of BP neural network.

The measurement results are all in good agreement with the nine tested points as shown in Figure 12. The actual AE source locations are the "×," the calculated coordinates of algebra algorithm are the "×," and the output results of BP network are "+." The results of AE source localization using different algorithm almost matched the test points uniformly. The maximum error of the test points on the coordinate axis is only 4.3 mm, and the maximum error of the four test points in the quadrant is 6.4 mm. The accuracy of the AE source localization is excellent with the small area array. It is hard to ensure the high accuracy when the monitoring area is enlarged, because the amplitude of stress wave attenuates with the long distance of propagation. Therefore, an image of sensor network consisting of some sensor arrays is presented for large structures, as shown in Figure 13. The test points in Array I have been measured, so the test points in similar parts such as Array II, Array III, and Array IV are also able to be exactly identified. The only test points in Array V needed extra measure because of the different distributions of the sensor array. This part of work will be achieved in the next research.

## Conclusion

In this article, the AE source is identified based on an intelligent algorithm with FOAES embedded in a CFRP plate. Calibration experiments of the FOAES show that it is better suited to detect the low frequency of stress wave than the PZT sensor. The experiments of

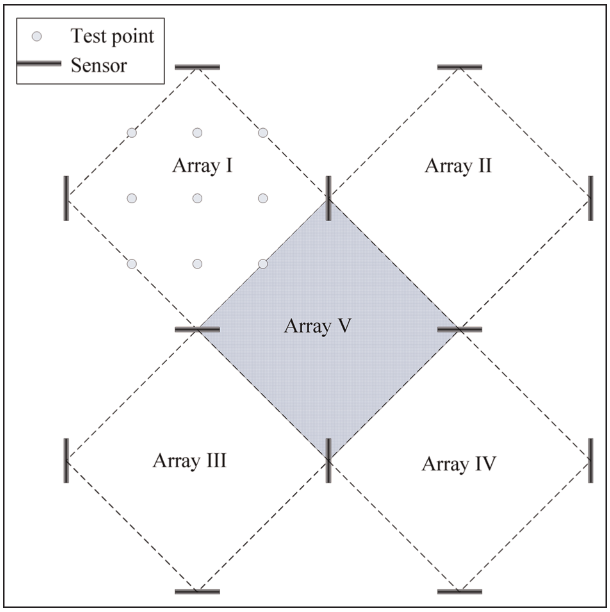


**Figure 13.** An imagine of sensor network for large structures.

AE source localization are achieved in isotropic plate with surface-mounted FOAESs distributed as a square array. The intelligent algorithm of BP neural network reduces the nonlinear errors and is suitable for any sensor array. The diamond array was integrated into CFRP plate for prediction of AE source location using the intelligent algorithm, which presented the trend of development of smart materials and structures in the future.

## Funding

This research received no specific grant from any funding agency in the public, commercial, or not-for-profit sectors.

## References

1. Mustapha S and Ye L. Debonding detection in composite sandwich structures based on guided waves. *AIAA J* 2012; 50(8): 1697–1706.
2. Kundu T, Das S, Martin SA, et al. Locating point of impact in anisotropic fiber reinforced composite plates. *Ultrasonics* 2008; 48(3): 193–201.
3. Koabaz M, Hajzargarbashi T, Kundu T, et al. Locating the acoustic source in an anisotropic plate. *Struct Health Monit* 2012; 11(3): 315–323.
4. Aljets D, Chong A, Wilcox S, et al. Acoustic emission source location on large plate-like structures using a local triangular sensor array. *Mech Syst Signal Pr* 2012; 30: 91–102.
5. Ciampa F and Meo M. A new algorithm for acoustic emission localization and flexural group velocity determination in anisotropic structures. *Compos Part A: Appl S* 2010; 41(12): 1777–1786.
6. Fu T, Liu Y, Li Q, et al. Fiber optic acoustic emission sensor and its applications in the structural health monitoring of CFRP materials. *Opt Laser Eng* 2009; 47(10): 1056–1062.
7. Leng J and Asundi A. Structural health monitoring of smart composite materials by using EFPI and FBG sensors. *Sensor Actuat A: Phys* 2003; 103(3): 330–340.
8. Leng J and Asundi A. Non-destructive evaluation of smart materials by using extrinsic Fabry-Perot interferometer and fiber Bragg grating sensors. *NDT&E Int* 2002; 35(4): 273–276.
9. Ho MP, Lau KT, Au HY, et al. Structural health monitoring of an asymmetrical SMA reinforced composite using embedded FBG sensors. *Smart Mater Struct* 2013; 22(12): 5015–5021.
10. Kahandawa GC, Epaarachchi JA, Wang H, et al. Use of fixed wavelength Fibre-Bragg Grating (FBG) filters to capture time domain data from the distorted spectrum of an embedded FBG sensor to estimate strain with an artificial neural network. *Sensor Actuat A: Phys* 2013; 194: 1–7.
11. Su Z and Ye L. A fast damage locating approach using digital damage fingerprints extracted from Lamb wave signals. *Smart Mater Struct* 2005; 14(5): 1047–1054.
12. Deng AD, Zhang XD, Tang JN, et al. Localization of acoustic emission source based on chaotic neural networks. *Appl Math Inf Sci* 2012; 6(3): 713–719.
13. Su Z and Ye L. Quantitative damage prediction for composite laminates based on wave propagation and artificial neural networks. *Struct Health Monit* 2005; 4(1): 57–66.
14. Su Z, Ling H-Y, Zhou L-M, et al. Efficiency of genetic algorithms and artificial neural networks for evaluating delamination in composite structures using fibre Bragg grating sensors. *Smart Mater Struct* 2005; 14(6): 1541–1553.
15. Coverley PT and Staszewski WJ. Impact damage location in composite structures using optimized sensor triangulation procedure. *Smart Mater Struct* 2003; 12(5): 795–803.
16. Chen R, Fernando GF, Butler T, et al. A novel ultrasound fibre optic sensor based on a fused-tapered optical fibre coupler. *Meas Sci Technol* 2004; 15: 1490–1495.
17. Chen R, Bradshaw T, Burns J, et al. Linear location of acoustic emission using a pair of novel fibre optic sensors. *Meas Sci Technol* 2006; 17: 2313–2318.
18. Fu T, Liu Y, Lau KT, et al. Impact source identification in a carbon fiber reinforced polymer plate by using embedded fiber optic acoustic emission sensors. *Compos Part B: Eng* 2014; 66: 420–429.
19. Su Y, Yuan S and Zhang B. Impact localization for composite based on acoustic emission and neural networks. *Transducer Microsyst Technol* 2009; 28(9): 56–61.
20. Lam PM, Lau KT, Ling HY, et al. Acousto-ultrasonic sensing for delaminated GFRP composites using an embedded FBG sensor. *Opt Laser Eng* 2009; 47: 1049–1055.
21. Hecht-Nielsen R. Kolmogorov's mapping neural network existence theorem. In: Proc IEEE conference, *Annu Int Conf Neural Netw* 1987; 3: 11–14.
22. Kirkby E, de Oliveira R, Michaud V, et al. Impact localisation with FBG for a self-healing carbon fibre composite structure. *Compos Struct* 2011; 94: 8–14.